

# An adaptive synchroextracting transform for the analysis of noise contaminated multi-component nonstationary signals

Jiaxin Li<sup>1</sup>, David Mba<sup>2</sup>, Xiaochuan Li<sup>3</sup>, Yajun Shang<sup>1</sup>, Shuai He<sup>1</sup> and Tian Ran Lin<sup>1,\*</sup>

<sup>1</sup> Center for Structural Acoustics and Machine Fault Diagnosis, Qingdao University of Technology, Qingdao 266520, China

<sup>2</sup> University of the Arts, London

<sup>3</sup> School of Electrical Engineering and Automation, Hefei University of Technology

\*Corresponding Author: trlin@qut.edu.cn

**Abstract:** The Synchro-Extracting Transform technique (SET) can capture the changing dynamic in a non-stationary signal which can be applied for fault diagnosis of rotating machinery operating under varying speed or/and load conditions. However, the time frequency representation (TFR) of a signal produced by SET can be affected by noise contained in the signal, which can largely reduce the accuracy of fault diagnosis. This paper addresses this drawback and presents a new extraction operator to improve the energy concentration of the TFR of a noise contaminated multi-component signal by using an adaptive ridge curve identification process together with SET. The adaptive ridge curve extraction is deployed to extract the signal components of a multi-component signal via an iterative approach. The effectiveness of the algorithm is verified using one set of simulated noise-added signals and two sets of experimental bearing and gearbox defect signals. The result shows that the proposed technique can accurately identify the fault components from noise contaminated multi-component non-stationary machine defect signals.

**Keywords:** nonstationary signal; time-frequency analysis; synchroextracting transform; ridge curve identification; fault diagnosis

## 1. Introduction

Critical components in the power transmission system of machinery such as rolling element bearings and gearboxes are prone to mechanical vulnerability under harsh continuous operation condition, which can lead to unexpected machine breakdown and associated financial losses [1, 2]. Condition monitoring (CM) techniques are an effective means to monitor, predict and alleviate unexpected machine failure. However, due to changing speed and load conditions during the machine operation, CM data/signals often demonstrate amplitude modulated (AM) and/or frequency modulated (FM) characteristics, which pose a challenge in the signal analysis for an accurate fault diagnosis using the traditional time or frequency analysis techniques [3, 4].

Time-frequency analysis (TFA) techniques are effective tools to characterize the time-varying features in a non-stationary signal [5]. Linear TFAs, such as short-time Fourier transform (STFT) and wavelet transform (WT), are characterized by the inner product between a signal and a moving time window function or kernel functions. However, restricted by Heisenberg uncertainty principle, STFT and WT cannot produce an accurate resolution in both time and frequency domains simultaneously. To overcome

this limitation, Daubechies et al. [6] proposed a synchrosqueezing transform based on the wavelet transform framework, termed as the SWT technique. An alternative synchrosqueezing transform (SST) technique was latter proposed by Thakur et al. [7] based on a STFT framework which can effectively extract the instantaneous frequencies (IFs) from a multi-component AM-FM signal. However, it has been pointed out by Iatsenko et al. [8] that synchrosqueezing transform (SST) can result in leakage of TF energy into other frequencies in the form of spiky TF support, and the noise contained in the signal can also be reassigned into the TFR of the signal.

Inspired by the success of SST, Yu et al. [9] proposed a so-called synchroextracting transform (SET) technique to extract the TF coefficients directly from the estimated IF so that the transform can retain the signal reconstruction ability of the STFT while removing the low-energy noise interference. Nonetheless, SET implicitly assumes that the signal is a slow time varying signal. This implies that the technique is not effective when dealing with strong non-stationary signals. A multi-synchrosqueezing transform (MSST) [10] was then proposed to overcome the diffused energy problem in a TFA by employing a multiple iterative process together with SST. MSST reassigns the TF coefficients of SST to the TF trajectories to produce an energy concentrated TFR, though the noise in the signal would also be squeezed and becomes severe after several iteration processes leading to a low readability of TFR. Yu et al. [11] further introduced a local maximum synchrosqueezing transform (LMSST) to generate a high energy concentrated TFR. The algorithm uses the TF energy matrix of the local maximum positions instead of the estimated IF to suppress the noise interference and to improve the readability of TFR [12]. A drawback of the algorithm is that the assignment operator in the transform is based on the local maximum energy coefficient in the TF energy matrix which needs prior knowledge.

Ridge curve identification is an effective technique in dealing with noisy signals by extracting the components of interest individually from a multi-component signal [13-20]. For instance, Peng et al. [16] combined the ridge curve identification with polynomial chirplet transform (PCT) to improve the TF energy concentration and established an iterative termination condition using the Rényi entropy. Whereas in Refs. [21] and [22], the instantaneous frequencies (IFs) were estimated by time-frequency peak detection, the spline chirp transform and the generalized warbler transform respectively. The general parametric TFA technique proposed in Ref. [23] also uses a similar approach to estimate the instantaneous frequencies for the corresponding parameter estimation. However, manual intervention is still required in the instantaneous frequency estimation process of multi-component signals using methods presented in the above-mentioned works. This has prompted the development of an adaptive algorithm presented in this paper.

An adaptive signal analysis technique based on ridge curve identification and SET is proposed in this paper as an automated approach to signal analysis of noise contaminated multi-component non-stationary signals without the pre-requisite knowledge of the signals. The remainder of the paper is organized as follows: In Section 2, the theoretical base of SET technique is reviewed. Section 3 elaborates the detailed

procedure of the proposed method and the framework. Numerical and experimental validations are provided in Sections 4 and 5, respectively. Conclusions are drawn in Section 6.

## 2. An improved synchroextracting transform

The main motivation of the proposed improved synchroextracting transform is to construct a new extraction operator via the ridge curve identification. The construction of the new operator is determined by adaptive ridge curve identification. The adaptive ridge extraction algorithm does not need to artificially determine the number of ridge extraction and can reduce interference items as far as possible on the premise of ensuring effective signal information. The flow chart of the ISET algorithm is shown below (see Fig. 1):

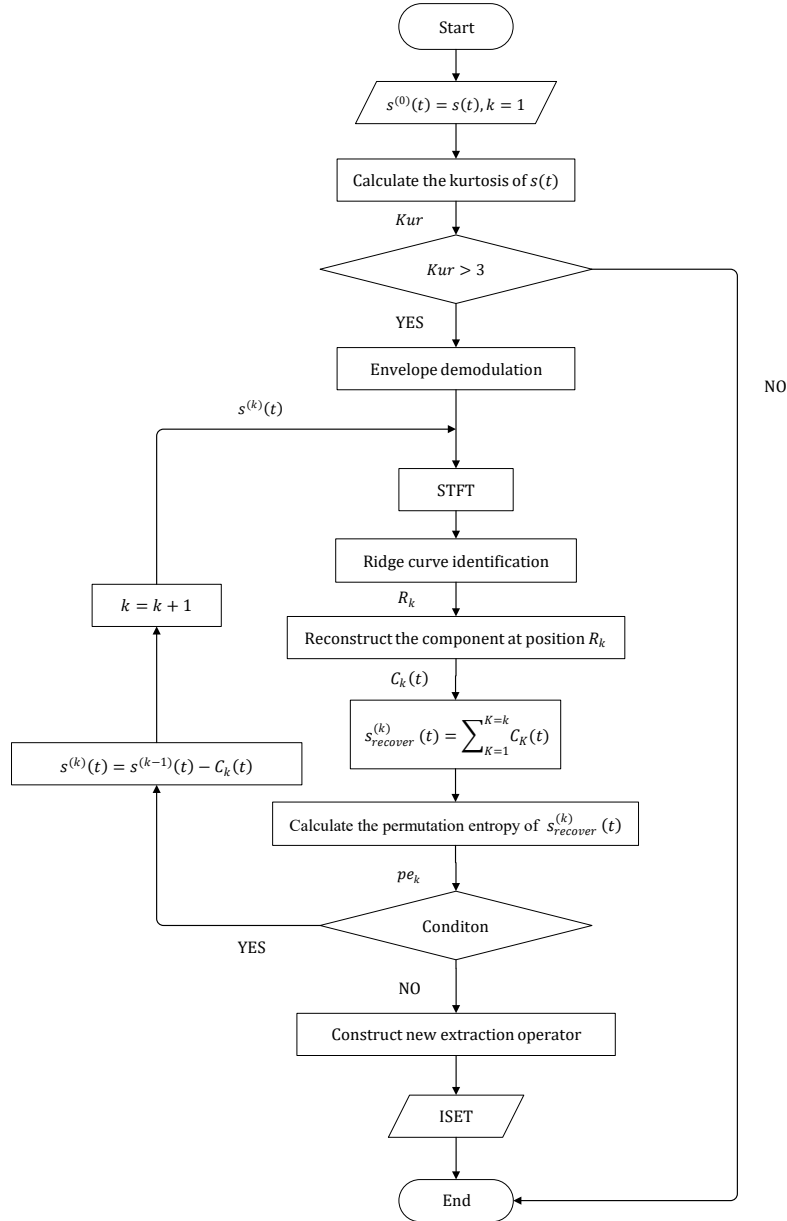


Figure 1. The flowchart of the proposed adaptive algorithm.

## 2.1 A theoretical background of the synchroextracting transform

For a given signal  $s(u) \in L^2(\mathbb{R})$ , the STFT of the signal considering an additional phase shift  $e^{-i\omega t}$  is [9]:

$$STFT(t, \omega) = \int_{-\infty}^{+\infty} g(u-t)s(u)e^{-i\omega(u-t)}du, \quad (1)$$

where  $g(u-t)$  is a moving time window;  $\omega$  is the angular frequency.

Let  $g_\omega(u) = g(u-t)e^{i\omega(u-t)}$ , according to Parseval's theorem, Eq. (1) can be re-expressed in the frequency domain as

$$STFT(t, \omega) = \frac{1}{2\pi} \int_{-\infty}^{+\infty} G_\omega^*(\xi) \cdot S(\xi) d\xi, \quad (2)$$

where  $*$  denotes a complex conjugation,  $G_\omega(\xi)$  and  $S(\xi)$  are the Fourier transform of  $g_\omega(u)$  and  $s(u)$  respectively. Then, we can have:

$$G_\omega(\xi) = \int_{-\infty}^{+\infty} g(u-t)e^{i\omega(u-t)}e^{-i\xi u}du. \quad (3)$$

Let  $u-t = \tau$ , Eq. (3) can be rewritten as:

$$G_\omega(\xi) = e^{-i\xi t} \int_{-\infty}^{+\infty} g(\tau)e^{-i(\xi-\omega)\tau}d\tau = e^{-i\xi t}G(\xi-\omega), \quad (4)$$

where  $G(\xi-\omega)$  is the Fourier transform of the moving time window  $g(u-t)$ . Substituting Eq. (4) into Eq. (2), the STFT of  $s(u)$  can be re-expressed as:

$$STFT(t, \omega) = \frac{1}{2\pi} \int_{-\infty}^{+\infty} G(\xi-\omega) \cdot S(\xi) \cdot e^{i\xi t} d\xi. \quad (5)$$

Noting that the Fourier transform of a purely harmonic signal  $s(t) = A \cdot e^{i\omega_0 t}$  is:

$$S(\xi) = 2\pi A \cdot \delta(\xi - \omega_0). \quad (6)$$

Substituting Eq. (6) into Eq. (5), we have:

$$STFT(t, \omega) = A \cdot G(\omega - \omega_0) \cdot e^{i\omega_0 t}. \quad (7)$$

By differentiating (7) with respect to time to have:

$$\omega_0(t, \omega) = \frac{\partial_t STFT(t, \omega)}{iSTFT(t, \omega)}, \quad (8)$$

where  $\omega_0$  is the estimated two-dimensional instantaneous frequency (IF).

SET extracts the TF coefficients of  $STFT(t, \omega)$  only at the IF trajectory  $\omega = \omega_0$  by using a synchro-extracting operator  $SEO(t, \omega) = \delta(\omega - \omega_0(t, \omega))$  together with STFT as:

$$SET(t, \omega) = STFT(t, \omega) * SEO(t, \omega). \quad (9)$$

## 2.2 An improved synchroextracting transform based on ridge curve identification

The transform operator  $SEO(t, \omega)$  can effectively suppress the noise interference by retaining only the TF coefficients at  $\omega_0$  in the STFT. However, it has been pointed out in Ref. [24] that the SET operator cannot produce an accurate estimate of the IFs if the signal is characterized by strong frequency modulation or the signal is contaminated by strong noise. In contrast, a ridge curve identification is robust against the noise contamination in the IF estimation. As a result, this study binds the ridge curve identification with SET, and proposes a new extraction operator  $nSEO(t, \omega)$  as follows:

$$nSEO(t, \omega) = \delta\left(\omega - \sum_{k=1}^K R_k\right), \quad (10)$$

where  $\sum_{k=1}^K R_k$  is the estimated IF by ridge curve identification from the TFR calculated using STFT,  $K$  is the number of components to be extracted.

Using the new extraction operator, an improved synchroextracting transform can be obtained:

$$iSET(t, \omega) = STFT(t, \omega) * nSEO(t, \omega). \quad (11)$$

A dynamic path optimization-based ridge detection (DPORD) algorithm [13] is adopted in this study to extract the ridge components of a multi-component signal adaptively, which is implemented in two major steps. In the first step, it extracts the peaks in the  $TF(t, \omega)$  of the signal using the following:

$$\begin{cases} m_v(t): \begin{cases} [\partial_\omega |TF(t, \omega)|]_{\omega=m_v(t)} = 0 \\ [\partial_\omega^2 |TF(t, \omega)|]_{\omega=m_v(t)} < 0 \end{cases}, \\ Q_v(t) = |TF(t, m_v(t))| \quad (v = 1, 2, \dots, N_p) \end{cases} \quad (12)$$

where  $m_v(t)$  denotes the frequency at the peak position for each time instant,  $Q_v(t)$  represents the amplitudes of  $TF(t, m_v(t))$ , and  $N_p$  is the total number of peak points in the entire TF domain.

In the second step, the locations of the actual ridge points at each discrete time are identified from the peak points  $N_p$  based on the following process. Curve extraction selects a sequence of peak points corresponding to each individual component from all possible trajectories judging by a cost function which forms a specific ridge curve [13]. Specific median function,  $\text{med}(f(t))$  and interquartile range function,  $\text{IQR}(f(t))$  of an arbitrary function  $f(t)$  are defined in Ref. [13] to construct the cost function according to the signal characteristics as:

$$\text{med}(f(t)) = \text{perc}_{0.5}[f(t)], \quad (13)$$

and

$$\text{IQR}(f(t)) = \text{perc}_{0.75}[f(t)] - \text{perc}_{0.25}[f(t)], \quad (14)$$

where  $\text{perc}_p$  denotes the  $p$ th quantile of  $f(t)$ . The cost function is then constructed as:

$$F[\dots] = \log Q_v(t_n) - \alpha \left| \frac{\Delta m_v(t_n) - \text{med}(\Delta m_v)}{\text{IQR}(m_v)} \right| - \beta \left| \frac{m_v(t_n) - \text{med}(m_v)}{\text{IQR}(m_v)} \right|, \quad (15)$$

where  $\alpha$  and  $\beta$  are the adjustable parameters to suppress the atypical variation of the frequency difference between two subsequent peak positions of the ridge [13],  $\Delta m_v(t_n) = m_v(t_n) - m_v(t_{n-1})$ ,  $n = 1, \dots, N$ .

Thus, the ridge  $R_k$  can be constructed using the following:

$$R_k = \underset{\{m_1, m_2, \dots, m_N\}}{\text{argmax}} \sum_1^N F[t_n, Q_m(t_n), m_v(t_n), \text{med}(m_v), \text{IQR}(m_v), \text{med}(\Delta m_v), \text{IQR}(\Delta m_v)], \quad (16).$$

DPORD can effectively overcome the noise interference to accurately extract the ridges from a multi-component signal. However, the construction of the  $nSEO(t, \omega)$  requires the prior knowledge of the component number  $K$  to be extracted from the signal, which is usually unknown for signals acquired from practical industrial sources. This then prompts the development of an adaptive algorithm to be presented in the next section.

### 2.3 An adaptive ridge curve identification for multi-component signals

Ridge curve identification algorithm extracts components from a multi-component signal in sequence where the ridge having the maximum cost function value is extracted first, which will then be subtracted from the original signal to yield a residual signal for the next ridge extraction process. The process will terminate when the last component is extracted from the signal. Thus, a prior knowledge of the component number contained in the signal is essential for the process. Nevertheless, such information is usually unavailable for data from industrial sources. To overcome this practical restraint, this work proposes an adaptive algorithm based on the permutation entropy of the signal. Permutation entropy is an average entropy parameter measuring the complexity of a time series data where a higher entropy indicating a more complexity of the time series [25].

The detailed process of the adaptive algorithm is elaborated below:

**Step1:** Calculate the kurtosis value of a signal to determine whether it contains fault induced impulse components:

$$Kur = \frac{E(s(t) - u)^4}{\sigma^4}, \quad (17)$$

where  $E$  represents the expectation operator,  $s(t)$  is the input signal;  $u$  is the mean value of the signal  $s(t)$ ; and  $\sigma$  is the standard deviation of the signal.

**Step 2:** Judge whether a signal contains fault induced impulses using the following condition [26]:

$$Kur > 3. \quad (18)$$

**Step 3:** Extract the first (dominating) component  $C_1(t)$  from the signal using the ridge curve identification algorithm, and then subtract the component from the original signal to form a subtracted signal  $s^{(1)}(t)$  for the next extracting process.

**Step 4:** Reconstruct the signal  $s_{recover}^{(k)}(t)$  using the extracted component from the  $k$ th ridge extraction:

$$s_{recover}^{(k)}(t) = \sum_{K=1}^{K=k} C_K(t). \quad (19)$$

**Step 5:** Calculate the permutation entropy [25, 27]  $pe_k$  of the reconstructed signal  $s_{recover}^{(k)}(t)$ . A phase space reconstruction can be performed for  $s_{recover}^{(k)}(t)$ , resulting in the following matrix [25]:

$$\begin{bmatrix} s_{recover}^{(k)}(1) & s_{recover}^{(k)}(1+T) & \dots & s_{recover}^{(k)}(1+(m-1)T) \\ s_{recover}^{(k)}(2) & s_{recover}^{(k)}(2+T) & \dots & s_{recover}^{(k)}(2+(m-1)T) \\ \vdots & \vdots & \ddots & \vdots \\ s_{recover}^{(k)}(j) & s_{recover}^{(k)}(j+T) & \dots & s_{recover}^{(k)}(j+(m-1)T) \\ s_{recover}^{(k)}(M) & s_{recover}^{(k)}(M+T) & \dots & s_{recover}^{(k)}(M+(m-1)T) \end{bmatrix}, \quad (j = 1, 2, 3, \dots, M), \quad (20)$$

where  $m$  and  $T$  are the embedding dimension and delay time respectively,  $M = n - (m - 1)T$ . Each row of the matrix can be regarded as a reconstructed signal component, and the  $m$  vectors in the  $j$ th row are rearranged in an ascending order, i.e.,  $[s_{recover}^{(k)}(j + (i_1 - 1)T) \leq s_{recover}^{(k)}(j + (i_2 - 1)T) \leq \dots \leq s_{recover}^{(k)}(j + (i_m - 1)T)]$ , where  $i_1, i_2, \dots, i_m$  correspond to the position of each element in the row. According to Ref. [25], a preferable range of  $m = 3 \sim 7$  was suggested since a smaller value of  $m$  in the phase space reconstruction matrix will reduce its ability in detecting the mutability of the signal, while a larger  $m$  will substantially increase the computation time. As a result, after a few errors and trials,  $m = 6$  and  $T = 3$  (the delay time) are chosen in this work. Thus, any row vector yields a set of symbolic sequence:

$$S(j) = [i_1, i_2, \dots, i_m]. \quad (21)$$

**Step 6:** Calculate the probability distribution  $P_1, P_2, \dots, P_g, \sum_{g=1}^{m!} P_g = 1$  for all symbolic sequences, where  $P_g$  is the probability of occurrence of symbolic sequence obtained after the reconstruction of the time-domain signal  $s_{recover}^{(k)}$ . The permutation entropy of a time series is defined as:

$$pe_k = - \sum_{g=1}^{m!} P_g \ln P_g. \quad (22)$$

**Step 7:** The termination condition for the ridge extraction iteration is given as follows:

$$\text{Condition } \left| \frac{pe_k - pe_{k-1}}{pe_{k-1}} \right| < \epsilon, \quad k = 2, 3, 4, \dots, n \quad (23)$$

where  $\epsilon$  is a very small number.

The iteration stops when the permutation entropy result obtained from Step 6 satisfies the termination condition, otherwise Step 2 - Step 6 will be repeated on the subtracted signal to extract the next signal component until the termination condition is met. The term in the new extract operator as given by Eq. (10),  $\sum_{k=1}^K R_k$ , can be calculated from summation of the ridges extracted from the multi-component signal.

### 3. Numerical validation

A 5-component varying speed signal as given below is simulated in this study to examine the validity of the proposed adaptive algorithm:

$$\begin{cases} s_1(t) = 3\cos\left[2\pi\left(20t + 20t^2 - \frac{20}{3}t^3\right)\right], \\ s_2(t) = 2.5\sin\left[2\pi\left(40t + 40t^2 - \frac{40}{3}t^3\right)\right], \\ s_3(t) = 2\sin[2\pi(60t + 60t^2 - 20t^3)], \\ s_4(t) = 1.5\sin\left[2\pi\left(80t + 80t^2 - \frac{80}{3}t^3\right)\right], \\ s_5(t) = \sin\left[2\pi\left(100t + 100t^2 - \frac{100}{3}t^3\right)\right], \\ s(t) = s_1(t) + s_2(t) + s_3(t) + s_4(t) + s_5(t). \end{cases} \quad (24)$$

The amplitudes of the five signal components  $s_1(t)$ ,  $s_2(t)$ ,  $s_3(t)$ ,  $s_4(t)$ ,  $s_5(t)$  are in decreasing order to test the effectiveness of the proposed algorithm under the influence of noise contamination. The simulated signal is assumed to be sampled at a rate of 500 Hz and lasts for 2 seconds. The time waveform of the simulated signal is shown in Fig. 2(a), its frequency spectrum is shown in Fig. 2(b).

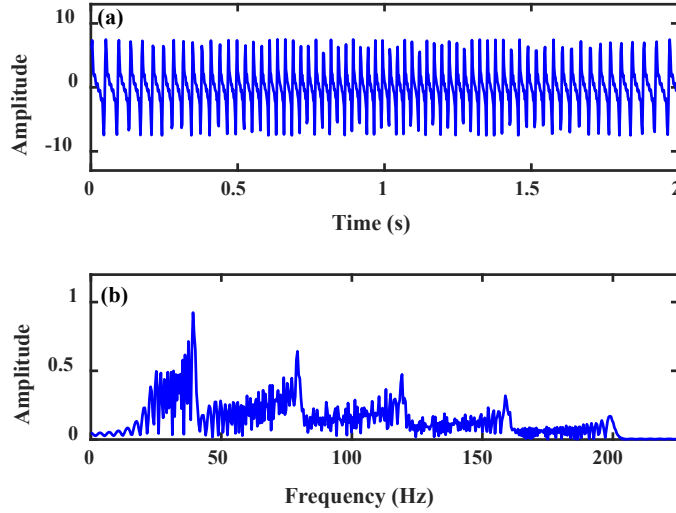


Figure 2. The simulated signal, (a) time waveform, and (b) frequency spectrum.

The simulated signal is analyzed first using the proposed ISET and SET for comparison, and the extracted IFs by the two techniques are shown in Fig. 3(a) and Fig. 3(b) respectively. It is shown the proposed ISET algorithm can effectively extract the IFs from the signal, whilst some interference terms are presented in the extracted IFs by SET, which can affect the clarification of the TFR. The situation can become much worst when there is noise presented in the signal.

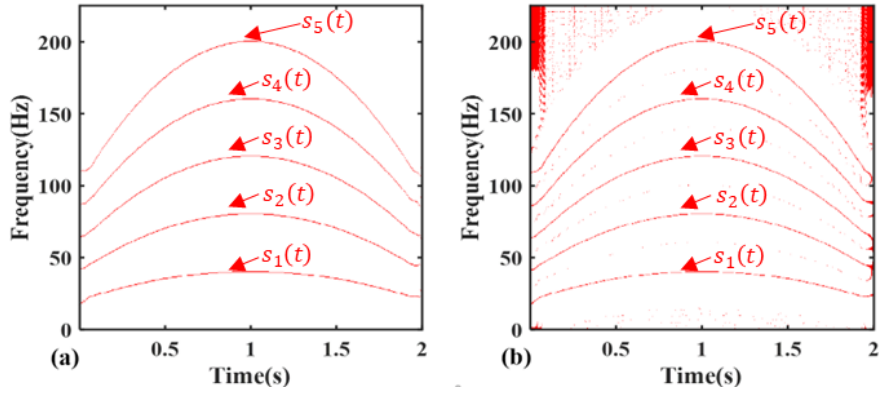


Figure 3. The extracted TFs from the simulated multi-component signal, (a) by ISET, (b) by SET.

To evaluate the effectiveness of the proposed algorithm under the noise interference, Gaussian white noise with different levels (2 dB, 0 dB, -2 dB and -4 dB) of signal-to-noise ratio (SNR) is added in sequence to the simulated signal in the following analysis until the largest signal component  $s_1(t)$  will also submerged under the added noise. The noise added signal having a SNR = 2 dB and its frequency spectrum are shown in Fig. 4. The extracted IFs using the proposed adaptive ISET algorithm is shown in Fig. 5. It is illustrated that except for the weakest component,  $s_5(t)$ , the IFs of the other four largest components can all be clearly extracted.

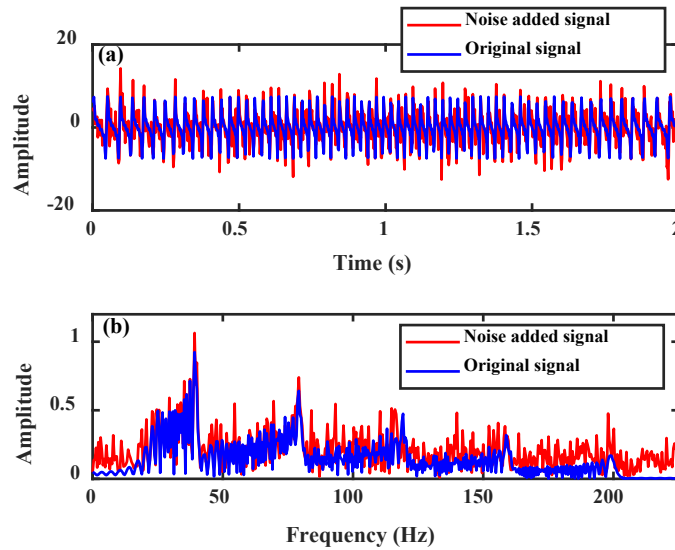


Figure 4. The noise added multi-component signal having a SNR = 2 dB, (a) the time waveform, (b) the frequency spectrum.

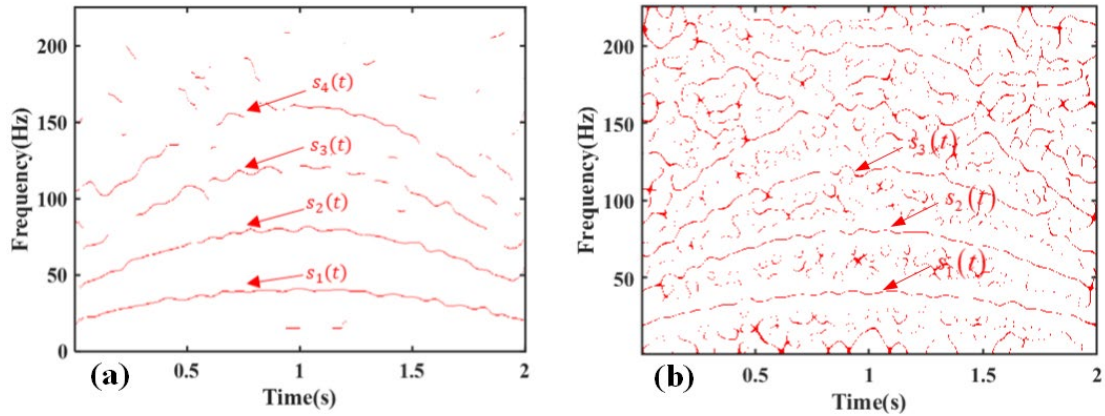


Figure 5. The extracted IFs of the noise added signal having SNR = 2 dB, (a) by ISET, (b) by SET.

Figure 6 compares the extracted IFs of the noise added signal having SNR=0 dB using both ISET and SET algorithms. It is shown in Fig. 6(a) that the two weakest signal components (i.e.,  $s_4(t)$  and  $s_5(t)$ ) have been submerged under the noise floor when the SNR of the added noise is 0 dB whilst the remaining three larger amplitude components are clearly detected using the proposed ISET. On the contrary, the useful signal components from the TFA result of SET are largely contaminated by the noise which are difficult to identify for a clear fault diagnosis as shown in Fig. 6(b).

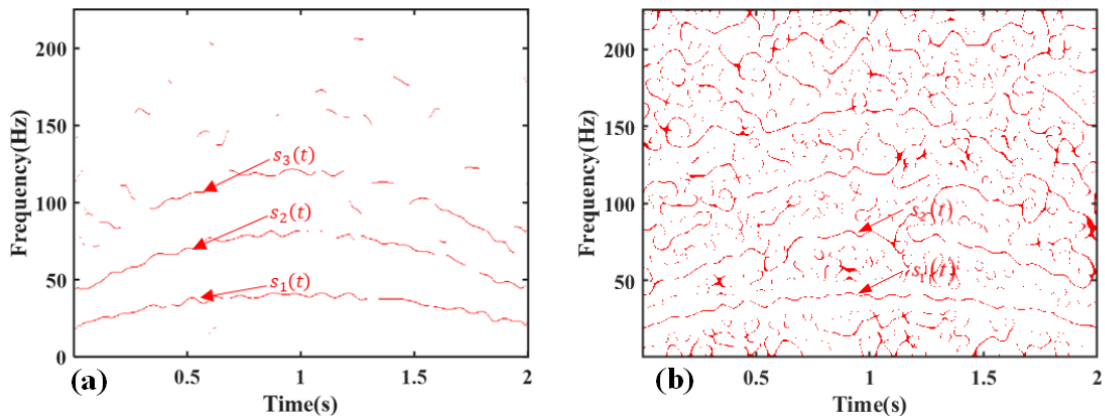


Figure 6. The IFs extracted of the noise added signal having SNR = 0 dB, (a) by ISET, (b) by SET.

Figure 7(a) displays the extracted IFs of the noise added signal having a SNR = -2 dB using the proposed ISET. It is found that only the two largest components  $s_1(t)$  and  $s_2(t)$  can still be extracted, the other components are all submerged under the interference of strong added noise. Similar to that of Fig. 7(b), the TFA result using SET is severely affected by the noise interference where the extracted TFs are hard to discern. Whereas Fig. 8(a) shows the extracted IFs of the noise added signal having SNR = -4 dB using ISET. It is found that only the largest signal component can still be detected using the proposed algorithm. When the SNR level of added white Gaussian noise is increased further, all the

signal components would be submerged under the noise floor and would not be detected from the analysis.

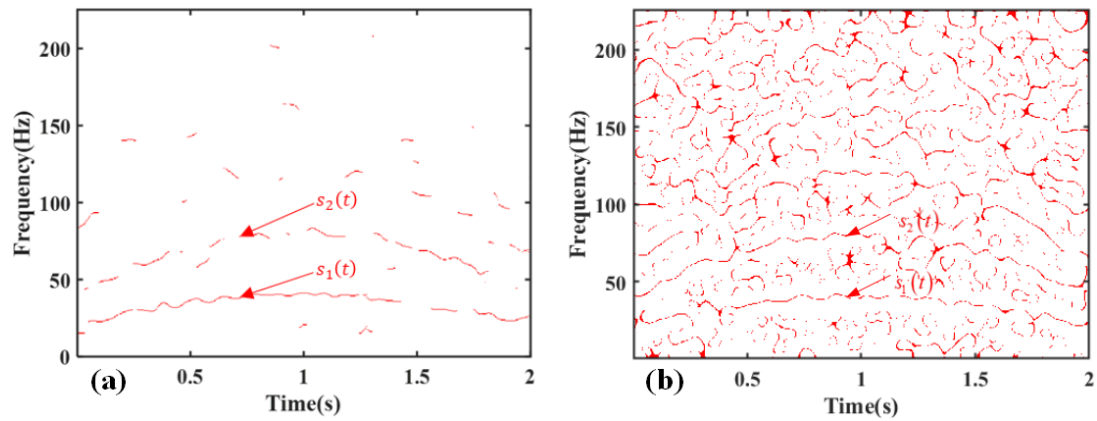


Figure 7. The IFs extracted of the noise added signal having SNR = -2 dB, (a) by ISET, (b) by SET.

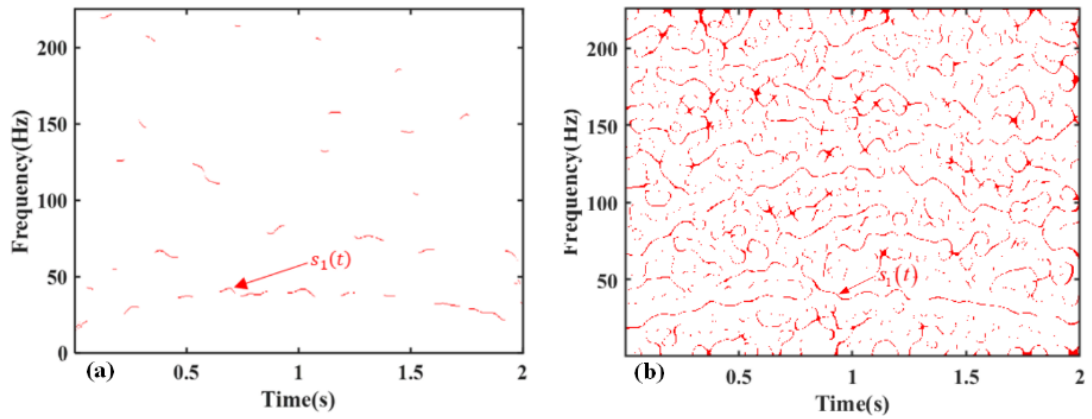


Figure 8. The IFs extracted of the noise added signal having SNR = -4 dB, (a) by ISET, (b) by SET.

Figure 9 compares the TFR results of the noise added signal having SNR = 0 dB using SET and ISET. The result demonstrates that the proposed ISET can adaptively extract the TF energy at the estimated IFs to produce a better time frequency result for a more accurate fault diagnosis of rotating machinery under the noise interference.

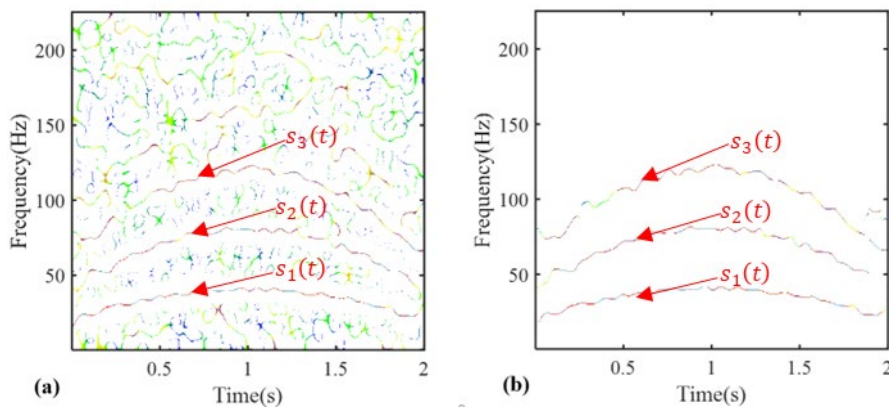


Figure 9. The TFR of the noise added signal having SNR = 0 dB, (a) SET, and (b) ISET.

To exemplify the effectiveness of the ISET in the analysis of noise contaminated non-stationary signals, the computation times of the technique in the analysis of signals with different SNRs are listed in Table I.

Table I A comparison of the computation time for different SNRs

SNR (dB)	2	0	-2	-4
Computation time (s)	0.95723	0.977415	0.994152	1.049082

## 4. Experimental validation

### 4.1 An evaluation using a non-stationary bearing defect data

The bearing data used in this analysis was acquired from an in-house Spectra Quest bearing fault simulator using a data acquisition system as shown in Fig.10. The type of the faulty bearing is an Er-16k bearing which is located at the righthand side of the test rig which structural parameters are listed in Table II. A graphical illustration of the defect bearing used in the experiment is shown in Fig. 11. The characteristic defect frequencies of the bearing are given in Table III. A B&K type 4370 accelerometer was installed on the top of the housing of the faulty bearing for the data acquisition as shown in the figure. A compound bearing fault including an outer ring defect, and inner ring defect and a defect on one of the rolling elements was simulated in the bearing experiment. The sampling frequency used in the experiment is 10 kHz, and the data length for each sample is 3 seconds. The motor speed during the experiment was varied from 1490 RPM to 1800 RPM and then back to 1490 RPM within the 3 seconds. The speed profile of the shaft during the experiment is shown in Fig. 12(a). The time waveform and the frequency spectrum of the bearing defect signal are shown in Figs. 12(b) and 12(c) respectively.

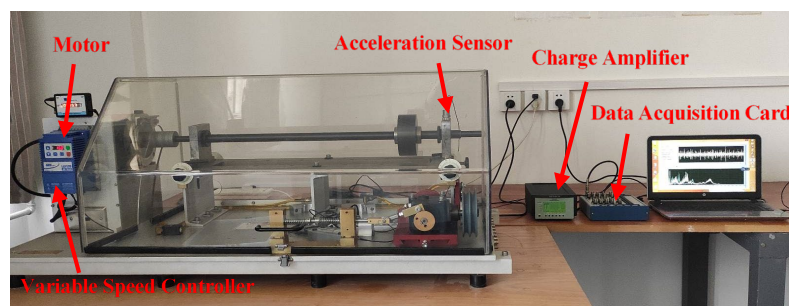


Figure10. The Spectra Quest bearing fault simulator.



Figure 11. A graphical illustration of the defect rolling element bearing used in the experiment.

Table II Structural parameters of the Er-16k bearing

Inner raceway diameter/(mm)	Pitch diameter / (mm)	Rolling element diameter / (mm)	Number of rolling elements	Contact angle / (°)
25.4	38.5	7.94	9	9.08

Table III Rolling element bearing characteristic frequencies

Inner ring ( $f_i$ )	Outer ring ( $f_o$ )	Rolling element ( $f_b$ )
$5.43f_r$	$3.572f_r$	$2.322f_r$

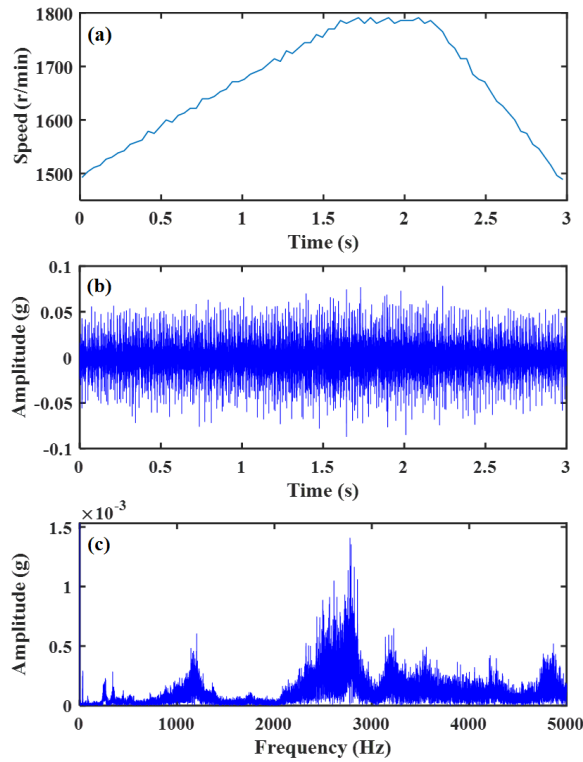


Figure 12. An illustration of the bearing experimental signal, (a) the shaft speed variation profile, (b) the time waveform of the bearing defect signal, and (c) the frequency spectrum.

The proposed ISET algorithm is then applied to analysis the time varying non-stationary bearing defect signal and the result is shown in Fig. 13(a) together with those using other commonly employed time-frequency algorithms such as SET, SST, RM and STFT for comparison.

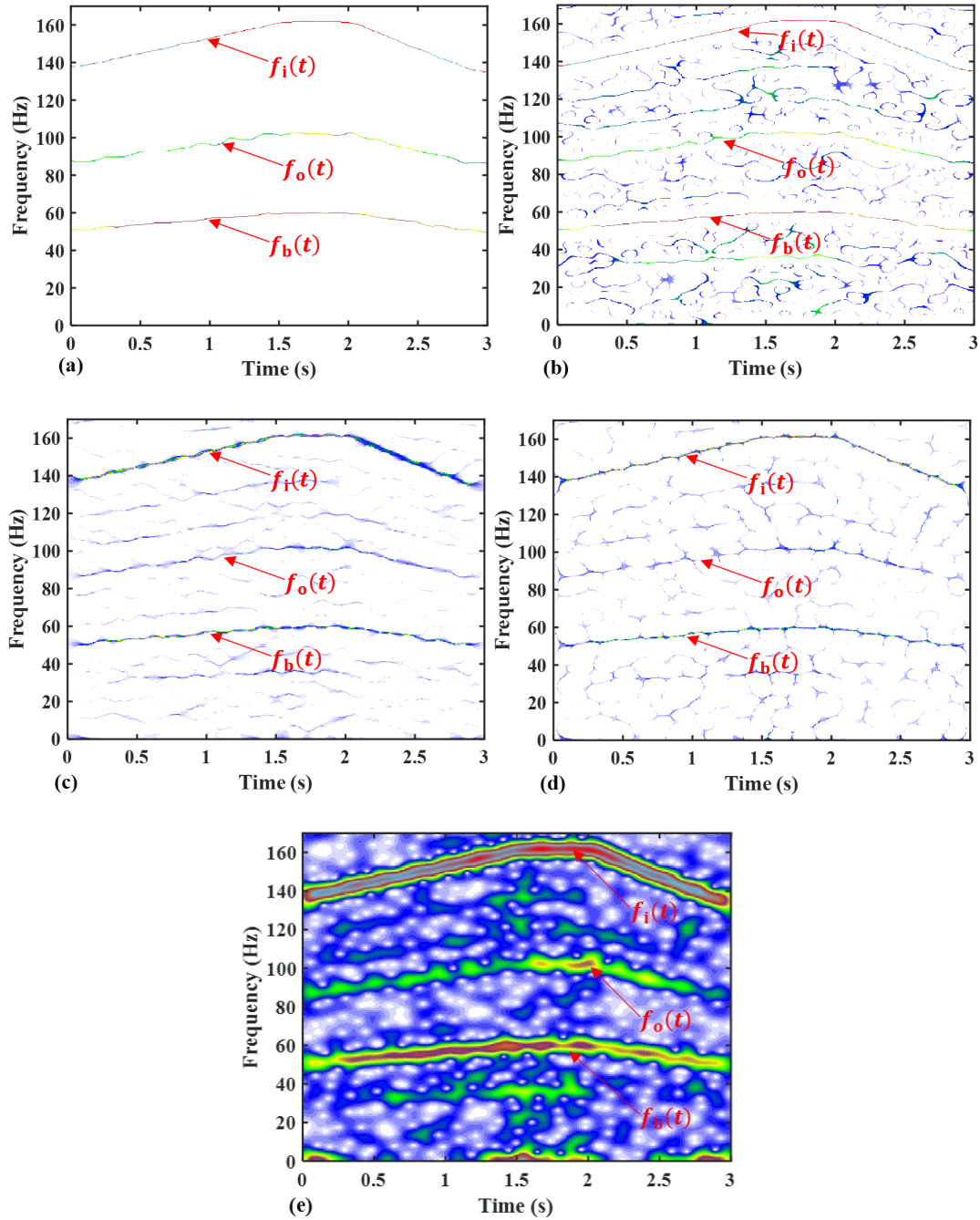


Figure 13. A comparison of TFR results using different time frequency analysis techniques, (a) ISET, (b) SET, (c) SST, (d) RM, and (e) STFT.

It is shown that the time frequency trajectories of all the defect frequency components (i.e.,  $f_i$ ,  $f_o$  and  $f_b$ ) are clearly shown in the result produced by the proposed ISET. Whereas there is noise interference in the TFR result using the other time frequency analysis techniques which may hinder the bearing fault diagnosis. A major advantage of the proposed adaptive ISET algorithm is that it can effectively eliminate

the noise interference contained in a condition monitoring data of unknown sources through the ridge curve extraction, and detect the defect signal component when its signal energy is higher than the background noise. This prospect thus inches the technique a step further towards the industrial application.

#### 4.2 An evaluation using a non-stationary planetary gearbox data

In this experiment, the defect data is acquired from an in-house [HOUDE METERS HD-CL-05 planetary gearbox test rig](#) as shown in Fig. 14. The test rig has two electric motors at each end of the rig, one as the main power source and the other as the load motor. The rig also has a planetary gearbox and a fixed axis gearbox for the gear fault experiment. There are two compound torque and speed sensors installed on the rig as shown in Fig. 14. The speed of the motor is controlled through a speed controller in the electronic control cabinet. A missing tooth fault of the sun gear as shown in Fig.15 is simulated in the experiment. The structural parameters of the planetary gearbox and the characteristic defect frequency of the sun gear are shown in Table IV and Table V.

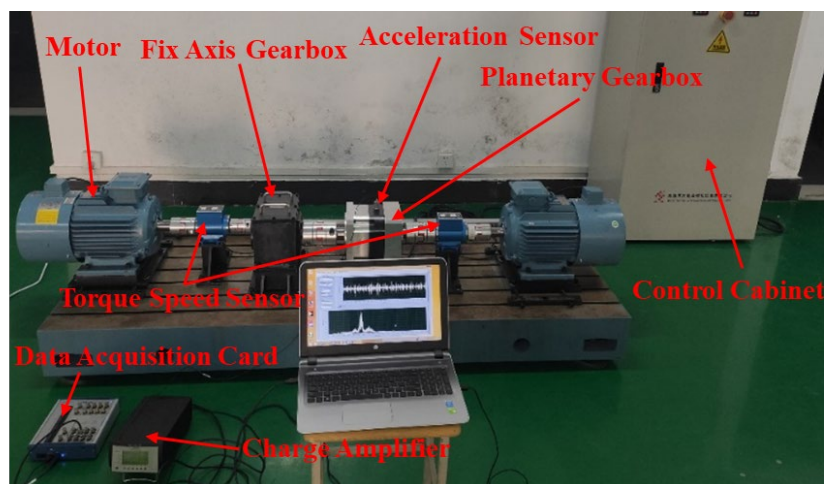


Figure 14. A graphic description of the planetary gearbox test rig.



Figure 15. A graphic illustration of the faulty sun gear with a missing tooth.

Table IV Planetary gearbox configuration parameters

Sun Gear (Number of Teeth)	Planet Gear (Number of Teeth)	Gear ring (Number of Teeth)	Number of Planet Gear
28	28	84	4

Table V Planetary gearbox characteristic frequencies

motor speed ( $f_r$ )	Sun gear rotation frequency ( $f_s^r$ )	Sun gear localized fault frequency ( $f_s$ )
21-30Hz	$f_r$	$3f_r$

A B&K4370 accelerometer is mounted on the casing of the planetary gearbox to acquire the vibration signal which was sampled at a sampling frequency of 10 kHz and a sampling length of 3 seconds. The speed of the motor shaft increases from 1260 RPM to 1800 RPM within the 3 seconds. The time waveform of the vibration signal from the experiment and the corresponding frequency spectrum are shown in Fig. 16.

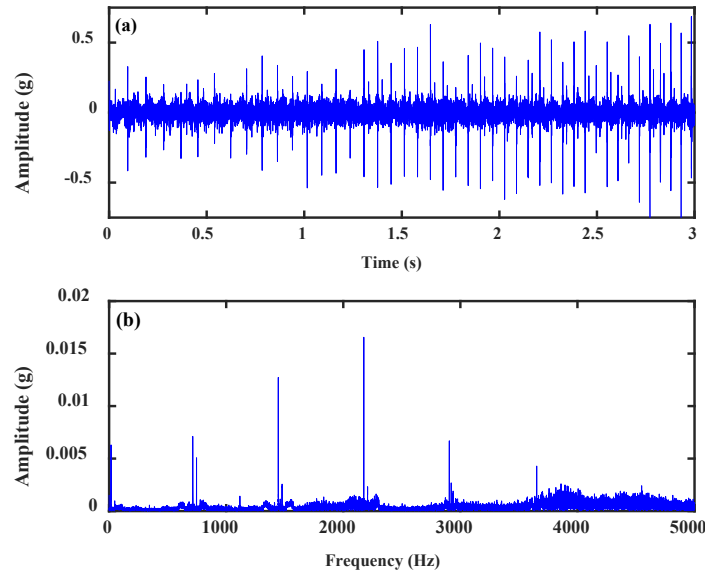


Figure 16. The vibration signal for the sun gear fault experiment, (a) the time waveform, (b) the frequency spectrum.

The proposed ISET technique is employed to extract the characteristic defect frequencies associating with the simulated sun gear fault, and the result is shown in Fig. 17 together with those from SET, SST, RM and STFT. It is shown that the ISET can extract both the fundamental sun gear defect frequency and its higher harmonics as well as the shaft rotating frequency and its higher harmonics adaptively to produce a clear readable TFR for an accurate fault diagnosis of planetary gearbox. On the other hand, results

obtained using the four comparative time-frequency analysis techniques are either contaminated by noise interference or having diffused energy distribution leading to inaccurate fault diagnosis.

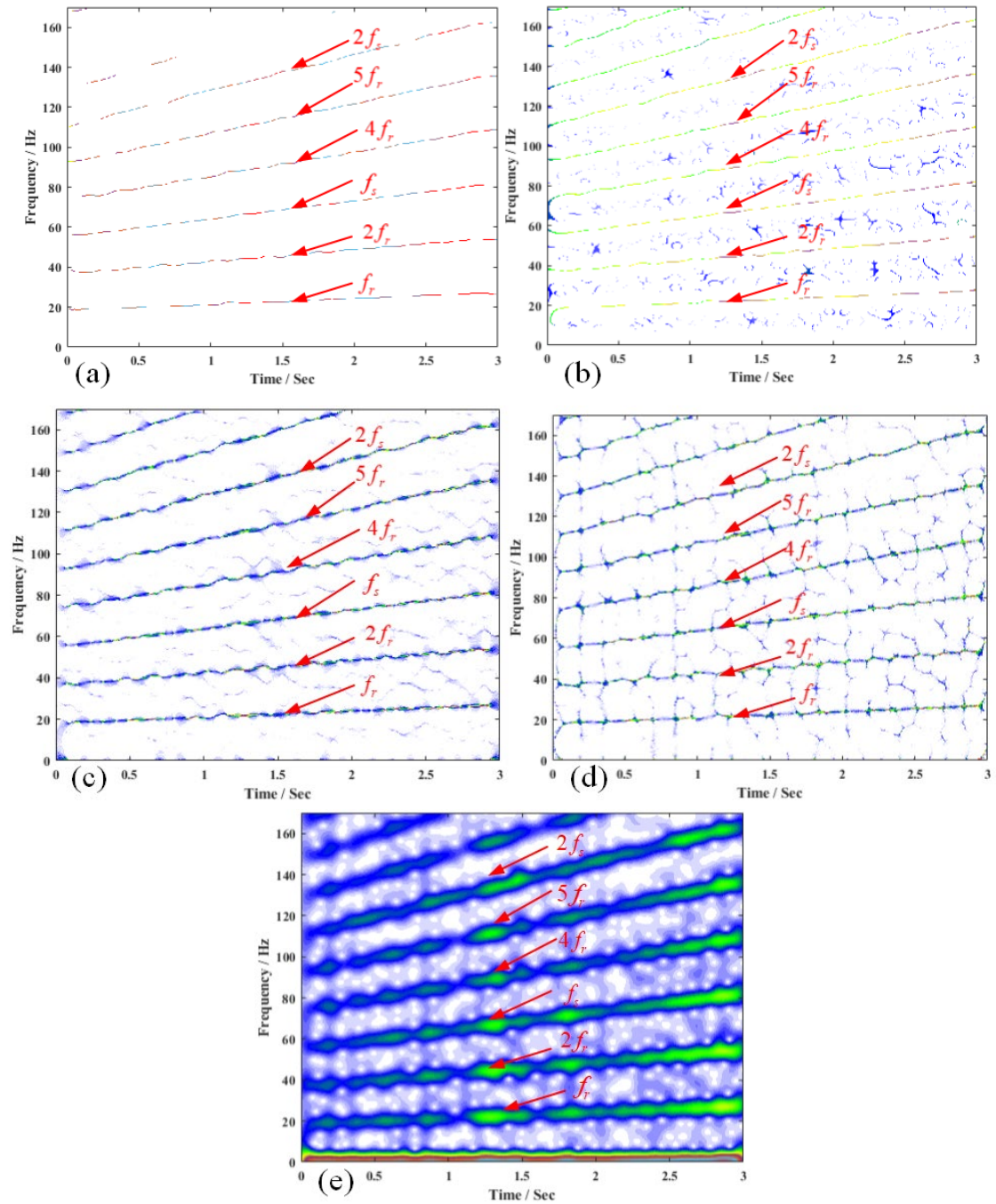


Figure17. A comparison of the TFR results for planetary gear fault diagnosis using different time frequency analysis techniques, (a) ISET, (b) SET, (c) SST, (d) RM, and (e) STFT.

## 5. Conclusion

In this study, we proposed a novel adaptive time frequency analysis algorithm for the analysis of non-stationary multi-component defect signals of rotating machinery under varying speed conditions. The effectiveness and robustness of the algorithm was validated using a set of noise added simulated multi-

component, non-stationary signals having different SNRs, and two sets of experimental data, one for a compound bearing defect and one for a planetary gearbox fault.

A main advance of the proposed algorithm is that it can effectively extract strong and weak components adaptively from a multi-component signal without the prior knowledge of the signal characteristic. It can also produce a clear readable time frequency representation from a noise contaminated non-stationary signal for an accurate fault diagnosis of a varying speed machine. The advantage of the proposed algorithm comparing to the commonly employed time frequency analysis techniques is clearly demonstrated in the analysis results presented in this work. A major limitation of this work is that the proposed technique has only been tested using either simulated or experimental data, its effectiveness needs to be examined in practical industrial applications, which constitutes to the future work.

## Acknowledgements

Financial supports from Qingdao Municipal Government through the Qingdao innovative leadership program (181219zhc) and the 111 project from the Ministry of Science and Technology of China (D21017) for this work are gratefully appreciated.

## References

1. K. Yu, T.R. Lin, J.W. Tan, A bearing fault diagnosis technique based on singular values of EEMD spatial condition matrix and Gath-Geva clustering, *Applied Acoustics*. 121 (2017) 33-45.
2. G. Yu, T.R. Lin, et al, Time-reassigned multisynchrosqueezing transform for bearing fault diagnosis of rotating machinery, *IEEE Trans. Indust. Electron.* 68 (2020) 1486-1496.
3. K. Yu, T.R. Lin, H. Ma, et al, A combined polynomial chirplet transform and synchroextracting technique for analyzing nonstationary signals of rotating machinery, *IEEE Trans. Instrum. Meas.* 69 (2019) 1505-1518.
4. J.P. Xing, T.R. Lin, D. Mba, A multi-component bearing fault diagnosis using fast iterative filtering technique, in *Proceedings of COMADEM 2019*, 3-5 September 2019, Huddersfield, UK.
5. F. Auger, P. Flandrin, Improving the readability of time-frequency and time-scale representations by the reassignment method, *IEEE Trans. Signal Process.* 43 (1995) 1068-1089.
6. I. Daubechies, J.F. Lu, H-T. Wu, Synchrosqueezed wavelet transforms: An empirical mode decomposition-like tool, *Applied and computational harmonic analysis*. 30 (2011) 243-261.
7. G. Thakur, H-T. Wu, Synchrosqueezing-based recovery of instantaneous frequency from nonuniform samples, *Siam. J. Math Anal.* 43 (2011) 2078-2095.
8. D. Iatsenko, P.V.E. McClintock, A. Stefanovska, Linear and synchrosqueezed time-frequency representations revisited: Overview, standards of use, resolution, reconstruction, concentration, and algorithms, *Digit. Signal Process.* 42 (2015) 1-26.
9. G. Yu, M.J. Yu, C.Y. Xu, Synchroextracting Transform, *IEEE Trans. Indust. Electron.* 64 (2017) 8042-8054.
10. G. Yu, Z.H. Wang, P. Zhao, Multisynchrosqueezing transform, *IEEE Trans. Indust. Electron.* 66 (2019) 5441-5455.

11. G. Yu, Z.H. Wang, P. Zhao, et al, Local maximum synchrosqueezing transform: an energy-concentrated time-frequency analysis tool, *Mech. Syst. Signal Process.* 117 (2019) 537-552.
12. Y. He, Z.N. Jiang, M.H. Hu, et al, Local maximum synchrosqueezing chirplet transform: an effective tool for strongly non-stationary signals of gas turbine, *IEEE Trans. Instrum. Meas.* 70 (2021) 1-14.
13. D. Iatsenko, P.V.E. McClintock, A. Stefanovska, Extraction of instantaneous frequencies from ridges in time–frequency representations of signals, *Signal Processing.* 125 (2016) 290-303.
14. Y.F. Li, Y. Yang, Y. Chen, et al, Iterative characteristic ridge extraction for bearing fault detection under variable rotational speed conditions, *ISA transactions.* 119 (2022): 172-183.
15. C. Li, V. Sanchez, G. Zurita, et al, Rolling element bearing defect detection using the generalized synchrosqueezing transform guided by time–frequency ridge enhancement, *ISA transactions.* 60 (2016) 274-284.
16. I. Djurović, L. Stanković, An algorithm for the Wigner distribution based instantaneous frequency estimation in a high noise environment, *Signal Processing.* 84 (2004) 631-643.
17. Z.K. Peng, G. Meng, F.L. Chu, et al, Polynomial chirplet transform with application to instantaneous frequency estimation, *IEEE Trans. Instrum. Meas.* 60 (2011) 3222-3229.
18. B. Barkat; B. Boashash. Instantaneous frequency estimation of polynomial FM signals using the peak of the PWVD: Statistical performance in the presence of additive Gaussian noise, *IEEE Trans. Signal Process.* 47 (1999) 2480-2490.
19. J. Urbanek, T. Barszcz, J. Antoni, A two-step procedure for estimation of instantaneous rotational speed with large fluctuations, *Mech. Syst. Signal Process.* 38 (2013) 96-102.
20. Meignen S, Oberlin T, Depalle P, et al, Adaptive multimode signal reconstruction from time–frequency representations, *Phil. Trans. R. Soc.* 374 (2016) 2065.
21. Y. Yang, Z.K. Peng, G. Meng, et al, Spline-kernelled chirplet transform for the analysis of signal with time-varying frequency and its application, *IEEE Trans. Ind. Electron.* 59 (2012) 1612-1621.
22. Y. Yang, Z.K. Peng, G. Meng, et al, Characterize highly oscillating frequency modulation using generalized warble transform, *Mech. Syst. Signal Process.* 26 (2012) 128-140.
23. Y. Yang, Z.K. Peng, X.J. Dong, et al, General parameterized time-frequency transform, *IEEE Trans. Signal Process.* 62 (2014) 2751-2764.
24. H.R. Dong, G. Yu, Comments on Synchroextracting transform: The theory analysis and comparisons with the synchrosqueezing transform, *Signal Processing.* 190 (2022): 108345.
25. C. Bandt, B. Pompe, Permutation entropy: a natural complexity measure for time series, *Physical review letters* .88 (2002): 174102.
26. W.S. Su, F.T. Wang, Z. Zhang, et al, Application of EMD denoising and spectral kurtosis in early fault diagnosis of rolling element bearings, *Journal of Vibration and Shock.* 29(3) (2010): 18-21.
27. Yan, Ruqiang, Yongbin Liu, and Robert X. Gao. Permutation entropy: A nonlinear statistical measure for status characterization of rotary machines, *Mechanical Systems and Signal Processing* 29 (2012): 474-484.